

Learning dictionary statistics from natural images

P. N. Loxley

Center for Nonlinear Studies and Theoretical Division,
Los Alamos National Laboratory,
Los Alamos, New Mexico, USA.

Abstract

A wavelet dictionary comprising a set of Gabor functions is learned from natural images using a sparse image code. Gabor functions describe the receptive field properties of simple cells in the primary visual cortex, and form a basis for efficiently coding natural image patches. Each Gabor function is completely specified by five parameters, and each parameter is treated as a random variable. I derive a learning rule and use it to learn a joint probability distribution over the Gabor parameters. Gabor parameters corresponding to receptive-field size and spatial frequency are found to be strongly correlated, and Pareto distributed: revealing that Gabor functions in the dictionary are scale invariant over a range of length scales. Parametric models of the joint probability distribution are estimated. Synthetic dictionaries sampled from these parametric models are shown to perform well on image-patch reconstruction, and highlight the importance of taking into account Gabor-parameter correlations. This approach generalizes uniform sampling of wavelet parameters, to sampling of wavelet parameters from non-uniform distributions learned from natural image data – thereby adapting wavelets to the statistics of the data.

1 Introduction

We know that simple cells in the primary visual cortex have spatially-localized receptive fields, and are tuned to stimulus features such as orientation, spatial frequency, and location in the visual field (Swindale, 1996). These simple

cells are the final stage of a mapping of stimulus features from the visual field to a retinotopic position on the surface of the primary visual cortex (Durbin and Mitchison, 1990). Various models have been proposed to explain how neural activity and visual experience could lead to development and organization of a cortical map (Swindale, 1996). For example, neural network models were used to describe the self-organization of orientation selectivity through a Hebbian learning rule with localized, oriented input patterns (von der Malsburg, 1973), or through a symmetry-breaking mechanism with uncorrelated random input (Linsker, 1986).

In addition to understanding the development and organization of a cortical map, it would be extremely useful to understand its function. The primary visual cortex represents an important stage in processing information along the visual pathway. Models capable of efficient coding of natural sensory data have been shown to develop realistic neural receptive fields that are adapted to the statistics of their input data (Olshausen and Field, 1996, 1997; Bell and Sejnowski, 1997). In this class of models, input consists of natural image patches – i.e., natural sensory data at the level of photoreceptors in the retina, and a Hebbian-like learning rule implementing an efficient coding strategy results in the adaptation of a set of basis functions analogous to the self-organization of orientation selectivity. The set of basis functions (called a *dictionary*) can be used to efficiently code and reconstruct natural image patches.

The output of an efficient coding model is an image code with fewer statistical dependencies than found between pixels in the input image. During the process of image formation light reflected from one or more physical objects is projected onto an image plane (Horn, 1986), so that particular combinations of image pixels (the pixel correlations) contain a lot of information about the underlying objects in a complicated way that depends on lighting, occlusion, viewpoint, and other effects (Ullman, 1996). Assuming different image sources to be largely independent of each other, the image code attempts to uncover the “causes” of an image in terms of statistically independent image sources (Bell and Sejnowski, 1997). These models work by making use of the high-order statistics of natural images, either through the assumed form of a prior distribution over output components of the image code (Olshausen and Field, 1997; Hyvärinen et. al., 2009), or through the assumed form of a nonlinear neural input-output function (Bell and Sejnowski, 1995).

A more traditional approach to efficient coding of image data is wavelet

analysis. Receptive fields of individual simple cells are well-described by the so-called *Gabor function* (Marcelja, 1980; also see references in Field, 1999), which is a function that has the property of minimum uncertainty for the simultaneous co-localization of a signal in space and in spatial frequency. Two-dimensional (2D) Gabor transforms were first used for image analysis and compression (Daugman, 1988), and for an early demonstration of a sparse image code that reduces entropy and decorrelates image pixels (Daugman, 1989). Lee later derived conditions for when a set of non-orthogonal 2D Gabor wavelets provides a complete image representation by generalizing the frame criterion for 1D wavelets (Lee, 1996). Application of this criterion led to the Gabor parameter quantizations (or sampling rates) necessary for generating a complete image code (Lee, 1996).

Efficient coding is possible due to the statistical properties of natural images (Field, 1994; Hyvärinen et. al., 2009). Strong pixel correlations in natural images lead to a high degree of redundancy: the distribution of natural images in pixel-space is non-uniform and concentrated in a small area (Field, 1994), while random images are uniformly distributed in pixel-space. An approximate $1/f$ Fourier amplitude spectrum (or $1/f^2$ power spectrum) completely describes the second-order statistics of pixel correlations in natural images. These correlations can be removed using either principal component analysis (PCA), or filter methods (Hyvärinen et. al., 2009). The Fourier phase spectrum conveys most of the image content and the higher-order pixel correlations (Field, 1994). Some of these correlations can be removed by seeking a linear transformation that generates an image code with sparse output components (Daugman, 1989; Bell and Sejnowski, 1995; Olshausen and Field, 1997; Hyvärinen et. al., 2009). In this case, each output component comes from a low-entropy marginal distribution, and therefore reduces the mutual information (the joint entropy remains approximately unchanged, while the individual entropies are minimized). Reducing the mutual information leads to output components that are closer to being statistically independent. Further pixel correlations can be removed with non-linear extensions of these models (Hyvärinen and Hoyer, 2000; Hyvärinen et. al., 2001; Köster and Hyvärinen, 2010).

For a learned dictionary to provide a useful basis for describing natural image patches, it must itself represent or reflect the statistics of natural images at some level. A natural question is: Can we extract this statistics in a meaningful way? Can we understand natural image statistics from the statistics of a dictionary; rather than from the statistics of image pixels, or

an image code?

In this Article, I attempt to address these questions by learning wavelet correlations and statistics for a dictionary of Gabor functions. Each Gabor function is completely specified by five parameters, and each parameter is treated as a random variable. The dictionary statistics is given by a learned joint probability distribution over the Gabor parameters. I then estimate parametric models for this learned joint distribution, and determine how well dictionaries generated from these parametric models perform compared to the learned dictionary. This approach generalizes that of Lee (1996): Here, Gabor parameters are sampled from non-uniform distributions learned from data, while Lee used a uniform sampling scheme.

The structure of this Article is as follows: In Section 2, the parametric Gabor dictionary is constructed, and a learning rule for the Gabor parameters is derived. In Section 3, this learning rule is used to learn the joint probability distribution of Gabor parameters, and statistical dependencies between pairs of Gabor parameters are characterized. Parametric models of the learned joint distribution are estimated in Sections 3 and 4, and synthetic dictionaries are then constructed and compared in Section 4 by sampling from these parametric models.

2 Model

The image model I apply is a linear generative model. Using the vector $\mathbf{r} = (x, y)$ to label the discrete pixel coordinates of image $I(\mathbf{r})$, each image is assumed to be generated by a sum of basis functions $g(\mathbf{r}, \mathbf{r}')$: one for each non-zero basis coefficient $a(\mathbf{r}')$, and Gaussian noise $N(\mathbf{r})$, as

$$I(\mathbf{r}) = \sum_{\mathbf{r}'} g(\mathbf{r}, \mathbf{r}') a(\mathbf{r}') + N(\mathbf{r}). \quad (1)$$

In order to investigate dictionary statistics I choose a parametric form for the dictionary g . Motivated by earlier work (Marcelja, 1980; Daugman, 1988, 1989; Lee, 1996), I start with the Gabor function:

$$G(\mathbf{r}) = \exp\left(\frac{-\tilde{y}^2 - \gamma^2 \tilde{x}^2}{2\sigma^2}\right) \cos\left(2\pi \frac{\tilde{y}}{\Lambda} + \varphi\right), \quad (2)$$

with

$$(\tilde{x}, \tilde{y}) = \begin{pmatrix} \cos \phi & -\sin \phi \\ \sin \phi & \cos \phi \end{pmatrix} \begin{pmatrix} x \\ y \end{pmatrix}, \quad (3)$$

giving a Gaussian-windowed sinusoid with five parameters $(\phi, \sigma, \gamma, \Lambda, \varphi)$. From the perspective of neuroscience, each of these parameters tells us something about the receptive field properties of simple cells in the primary visual cortex. A parameter value of $\gamma \neq 1$ means a simple cell responds more strongly to a visual stimulus given by a bar or an edge instead of a circular spot. In this case, the optimal stimulus response is given for a stimulus orientation ϕ . The parameters σ and Λ correspond to how well localized a receptive field is in space, and in spatial frequency $1/\Lambda$, respectively. The φ parameter corresponds to the simple-cell phase response.

To learn values for the Gabor parameters from natural images, I construct a parametric dictionary by generalizing the Gabor function in a straightforward way as

$$g(\mathbf{r}, \mathbf{r}') = \exp\left(\frac{-\tilde{y}^2 - \gamma(\mathbf{r}')^2 \tilde{x}^2}{2\sigma(\mathbf{r}')^2}\right) \cos\left(2\pi \frac{\tilde{y}}{\Lambda(\mathbf{r}')} + \varphi(\mathbf{r}')\right), \quad (4)$$

with

$$(\tilde{x}, \tilde{y}) = \begin{pmatrix} \cos \phi(\mathbf{r}') & -\sin \phi(\mathbf{r}') \\ \sin \phi(\mathbf{r}') & \cos \phi(\mathbf{r}') \end{pmatrix} \begin{pmatrix} x - x' \\ y - y' \end{pmatrix}. \quad (5)$$

Gabor functions uniformly tile space in this construction: at each discrete spatial position \mathbf{r} there is a Gabor function centered at $\mathbf{r} = \mathbf{r}'$ with a unique set of parameters $\phi(\mathbf{r}')$, $\sigma(\mathbf{r}')$, $\gamma(\mathbf{r}')$, $\Lambda(\mathbf{r}')$, and $\varphi(\mathbf{r}')$. Although it is the basis functions that are chosen to have a Gabor form, receptive fields (given by the responses of each $a(\mathbf{r})$ to inputs consisting of spots at every position) are similar in form to the basis functions (Olshausen and Field, 1996); and have essentially the same orientation, location, and spatial frequency tuning (Hyvärinen et. al., 2009).

Following Olshausen and Field (1997), and Lewicki and Olshausen (1999), the probability of generating a particular image I is assumed to be given by a latent variable model of the form:

$$P(I|\boldsymbol{\theta}) = \int da P(I|\boldsymbol{\theta}, a) P(a), \quad (6)$$

where a are the unobserved (latent) variables, and $\boldsymbol{\theta}(\mathbf{r}) = (\phi(\mathbf{r}), \sigma(\mathbf{r}), \gamma(\mathbf{r}), \Lambda(\mathbf{r}), \varphi(\mathbf{r}))$ is a vector of the five Gabor parameters. For the case of Gaussian noise with variance σ' : $P(I|\boldsymbol{\theta}, a) \propto \prod_{\mathbf{r}} \exp(-N(\mathbf{r})^2/2\sigma'^2)$; while the marginal distribution for a is assumed to be sparse and to factor: $P(a) \propto \prod_{\mathbf{r}} \exp(-\beta S(a(\mathbf{r})))$. Usual choices for $P(a)$ include the Cauchy distribution, i.e. $S(x) = \log(1 + x^2)$;

the “logistic” distribution, i.e. $S(x) = \log(\cosh x)$; or the Laplacian distribution, i.e. $S(x) = |x|$ (Hyvärinen et. al., 2009). In the present work, the Cauchy distribution is chosen.

Estimating parameters in a latent variable model can be done efficiently using the EM algorithm (Bishop, 2006). The E-step begins by inferring the latent variables a , given $\boldsymbol{\theta}$ and I . Using Bayes’ rule, $P(a|I, \boldsymbol{\theta})$ can be written as

$$P(a|I, \boldsymbol{\theta}) \propto P(I|\boldsymbol{\theta}, a)P(a). \quad (7)$$

Since the expectation over $P(a|I, \boldsymbol{\theta})$ cannot be evaluated analytically, a good estimate of the latent variables must be found. One approach (known as is to use the Maximum Posterior (MAP) estimate for a . Upon defining $E = -\log [P(I|\boldsymbol{\theta}, a)P(a)]$, and using Eq. (7) with the presented forms for $P(I|\boldsymbol{\theta}, a)$ and $P(a)$, this can be written as

$$\hat{a} = \arg \max_a P(a|I, \boldsymbol{\theta}), \quad (8)$$

$$= \arg \min_a E, \quad (9)$$

where

$$E = \sum_{\mathbf{r}} \left\{ \frac{1}{2} \left[I(\mathbf{r}) - \sum_{\mathbf{r}'} g(\mathbf{r}, \mathbf{r}') a(\mathbf{r}') \right]^2 + \lambda S(a(\mathbf{r})) \right\}, \quad (10)$$

with $\lambda = \sigma'^2 \beta$. Finding the MAP value for a therefore reduces to simultaneously minimizing the least-squares error and sparseness terms in Eq. (10). For the Cauchy distribution, this has been done using conjugate gradient descent (Olshausen and Field, 1996, 1997). For the Laplacian distribution, this is known as *basis pursuit denoising*; and many fast and efficient algorithms have recently been developed (see Goldstein and Osher, 2009, for example).

The M-step involves maximizing the average log-likelihood $\langle \log P(I|\boldsymbol{\theta}) \rangle$ with respect to the Gabor parameters $\boldsymbol{\theta}$. The average log-likelihood is the likelihood function given by Eq. (6), averaged over a batch of image patches. Maximizing this quantity is equivalent to minimizing the Kullback-Leibler divergence between the distribution of images in nature, and the distribution of images generated from the image model (Olshausen and Field, 1997).

Maximizing the log-likelihood is implemented using gradient ascent:

$$\Delta\theta_i(\mathbf{r}) = \eta_i \frac{\partial}{\partial\theta_i(\mathbf{r})} \langle \log P(I|\boldsymbol{\theta}) \rangle, \quad (11)$$

$$= \eta_i \left\langle \frac{1}{P(I|\boldsymbol{\theta})} \frac{\partial}{\partial\theta_i(\mathbf{r})} \sum_a P(I|\boldsymbol{\theta}, a) P(a) \right\rangle, \quad (12)$$

$$= \eta_i \left\langle \frac{1}{P(I|\boldsymbol{\theta})} \sum_a P(I|\boldsymbol{\theta}, a) P(a) \left(-\frac{\partial E}{\partial\theta_i(\mathbf{r})} \right) \right\rangle, \quad (13)$$

$$= -\eta_i \left\langle \sum_a P(a|\boldsymbol{\theta}, I) \frac{\partial E}{\partial\theta_i(\mathbf{r})} \right\rangle, \quad (14)$$

$$= -\eta_i \left\langle \left\langle \frac{\partial E}{\partial\theta_i(\mathbf{r})} \right\rangle_{P(a|\boldsymbol{\theta}, I)} \right\rangle, \quad (15)$$

where η_i are the learning rates, and E is given by Eq. (10). The gradient can be written as

$$\frac{\partial E}{\partial\theta_i(\mathbf{r})} = -a(\mathbf{r}) \sum_{\mathbf{r}'} r(\mathbf{r}') \frac{\partial g(\mathbf{r}', \mathbf{r})}{\partial\theta_i(\mathbf{r})}, \quad (16)$$

where the residual error $r(\mathbf{r})$ is defined as

$$r(\mathbf{r}) = I(\mathbf{r}) - \sum_{\mathbf{r}'} g(\mathbf{r}, \mathbf{r}') a(\mathbf{r}'). \quad (17)$$

Using these two expressions in Eq. (15) leads to

$$\Delta\theta_i(\mathbf{r}) = \eta_i \sum_{\mathbf{r}'} \frac{\partial g^T(\mathbf{r}, \mathbf{r}')}{\partial\theta_i(\mathbf{r})} \left\langle \langle a(\mathbf{r}) r(\mathbf{r}') \rangle_{P(a|\boldsymbol{\theta}, I)} \right\rangle, \quad (18)$$

where the partial derivatives for g are given in Append. A. Updating each Gabor parameter therefore requires the calculation of two expectations. The inner expectation in Eq. (18) is with respect to the posterior distribution $P(a|\boldsymbol{\theta}, I)$ given by Eq. (7), and is evaluated in the E-step. The outer expectation is an average over a batch of image patches. Evaluating both expectations, then adjusting each Gabor parameter according to Eq. (18), constitutes the M-step. The EM algorithm consists of alternating between the E-step and the M-step until convergence is reached (Bishop, 2006).

The approach outlined here allows modeling of Gaussian noise and an overcomplete basis. If the noise level is zero and the basis is complete, the E-step can be avoided, and the ICA learning rule follows. In this case, Eq. (1) can be inverted to give $a(\mathbf{r}) = \sum_{\mathbf{r}'} g(\mathbf{r}, \mathbf{r}')^{-1} I(\mathbf{r}')$, and the distribution $P(I|\boldsymbol{\theta}, a)$ in Eq. (6) becomes a delta-function. Performing the sum over a in Eq. (6) then yields $P(I|\boldsymbol{\theta}) = P(g^{-1}I)$. Maximizing this likelihood forms the basis of the FastICA algorithm discussed in Hyvärinen et. al. (2009).

In the presence of Gaussian noise or for an overcomplete basis, the E-step is usually performed either by sampling from $P(a|\boldsymbol{\theta}, I)$, or by using its MAP estimate from Eq. (8). For the case of the MAP approach, the learning rule in Eq. (18) becomes

$$\Delta\theta_i(\mathbf{r}) = \eta_i \sum_{\mathbf{r}'} \frac{\partial g^T(\mathbf{r}, \mathbf{r}')}{\partial \theta_i(\mathbf{r})} \langle \hat{a}(\mathbf{r}) \hat{r}(\mathbf{r}') \rangle, \quad (19)$$

where \hat{r} is the residual error from Eq. (17) with \hat{a} instead of a , and \hat{a} is the MAP estimate given by Eq. (8). This learning rule turns out to be similar in form to that of Olshausen et. al (2001), except the dictionary elements in g are now specialized to Gabor functions. The drawback of using MAP instead of sampling in the E-step is encountering a trivial solution given when both terms in Eq. (10) are minimized by a small value of a , and a large value of g ; such that $ga \sim I$. To avoid this solution, Olshausen and Field (1997) introduced a learning rule for the L_2 -norm of the basis functions. Here, I define

$$\tilde{L}_2(\mathbf{r}) = \sqrt{\sigma(\mathbf{r})^2}, \quad (20)$$

and avoid the trivial solution by supplementing Eq. (19) with the learning rule:

$$\tilde{L}_2(\mathbf{r})^{\text{new}} = \tilde{L}_2(\mathbf{r})^{\text{old}} \left[\frac{\langle \hat{a}(\mathbf{r})^2 \rangle}{\sigma_{\text{goal}}^2} \right]^\alpha, \quad (21)$$

to update the $\sigma(\mathbf{r})$ values.

3 Results

Now I apply the learning rules given by Eqs. (19)–(21) to a set of image patches of size 16×16 pixels ($N = 256$ pixels). A total of 10^6 image patches in batches of 100 were randomly selected from 10 images of natural scenes

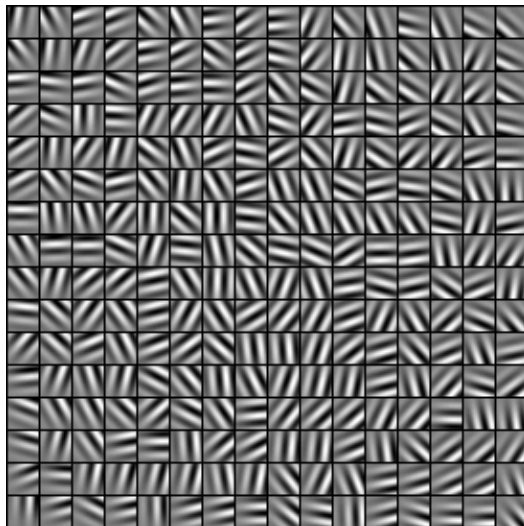


Figure 1: Initial dictionary of 256 Gabor basis functions. The parameters ϕ and φ were chosen at random from uniform distributions over 0 and π (for ϕ), and $-\pi$ and π (for φ). Other parameters were chosen as: $\gamma = 1$; $\sigma = 0.5\sqrt{N}$; and $\Lambda = 0.5\sqrt{N}$ (see text).

taken from *Sparsenet*. The image pre-processing includes both whitening and dimensionality reduction, as described in Olshausen and Field (1997). The MAP approach was used in the E-step with the Cauchy distribution and conjugate gradient descent in order to facilitate a close comparison with Olshausen’s and Field’s non-parametric dictionary.

The first objective is to demonstrate that the learning rules given by Eqs. (19)–(21) lead to a set of basis functions that are oriented, localized, and bandpass as originally shown in Olshausen and Field (1996). To demonstrate this, I start with the opposite case given by the initial dictionary in Fig. 1: each basis function is circularly symmetric, global in space (covering a whole image patch), and global in wavenumber space. The learned dictionary in Fig. 2 clearly shows the set of basis functions have become oriented, localized, and bandpass (see also Fig. 4). This dictionary is approximately 1.4-times over-complete: its singular values drop off sharply after about 180 dimensions.

To show that the learned parametric dictionary is approximately as effective as a non-parametric dictionary learned using *Sparsenet*, I compare

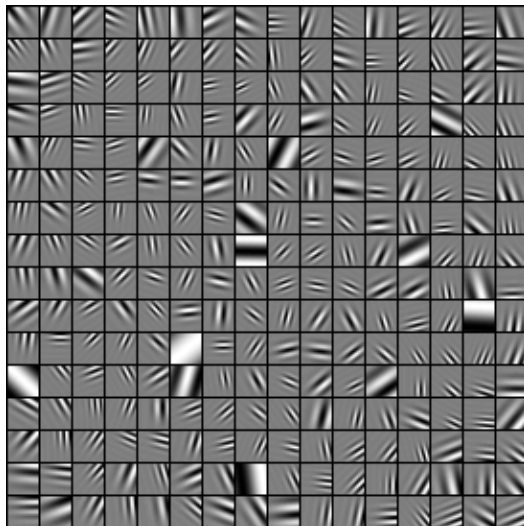


Figure 2: Learned dictionary of 256 Gabor basis functions. Statistics of the Gabor parameters are shown in Figs. 4 and 5.

image-patch reconstruction performance. For each of the dictionaries I compute the MAP value of a using Eqs. (9) and (10) for a test image patch chosen at random. I then find the patch reconstruction error given by $\frac{1}{2}|\mathbf{I} - \mathbf{g}\hat{\mathbf{a}}|^2$. I repeat this procedure for 300 test patches and take the average. This entire procedure is then repeated for different λ values to determine image-patch reconstruction performance at different sparseness levels. The mean reconstruction error at different sparseness levels is shown in Fig. 3. The sparseness norm for a single patch = $\sum_{\mathbf{r}} S(a(\mathbf{r})) / \sum_{\mathbf{r}} S(I(\mathbf{r}))$, and has a small value when λ is large and a is sparse. Averaging over all patches gives the mean sparseness norm plotted in Fig. 3. This figure shows that the learned dictionary performs significantly better than the initial dictionary, and has similar performance to the non-parametric dictionary. It also shows reconstruction performance degrading with increasing sparseness of a (i.e., decreasing mean sparseness norm), as expected.

Having established these benchmark results, the main aim of this work is to investigate and model the joint probability distribution of the learned Gabor parameters. Histograms of the learned Gabor parameters are shown in Fig. 4. I fitted continuous distributions to this data which are shown as the solid lines in each of the histogram plots. I removed 5 outliers from the

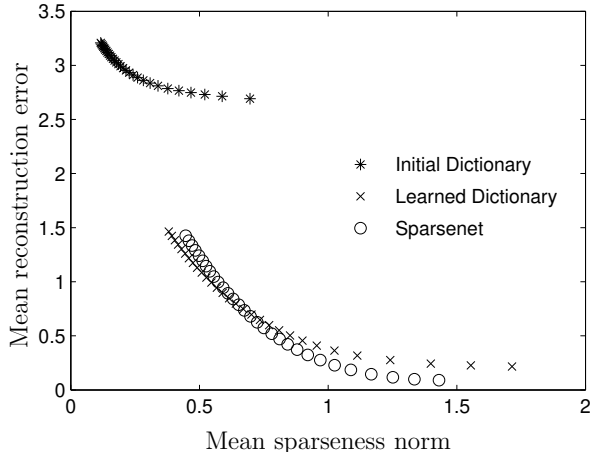


Figure 3: Mean reconstruction error for a set of 300 test-patch reconstructions at different sparseness levels (see text). Results from using the dictionary of initial values from Fig. 1 (Asterisks), the learned dictionary from Fig. 2 (Crosses), and a dictionary of non-parametric basis functions (Circles) learned using *Sparsenet*.

256 data points in order to generate these plots. The fitted distributions and their parameter estimates are given in Table 1; parameters with hats correspond to maximum-likelihood estimates.

The histograms in Fig. 4 are well-fitted by uniform, Pareto, and Gaussian univariate distributions. Isotropy in natural images is a reasonable first approximation (Hyvärinen et. al., 2009), so characterizing the orientation parameter ϕ with a uniform distribution seems appropriate. Similarly, the phase parameter φ appears to be uniformly distributed as in the initial dictionary. The aspect-ratio γ is Gaussian distributed with a mean < 1 , indicating a significant deviation from the unit aspect ratio of basis functions with circular symmetry. The two spatially-dependent parameters σ and Λ are each well-described by a Pareto distribution (Mardia, 1962) of the form

$$\mathcal{P}(x|\alpha, x_m) = \begin{cases} \alpha x_m^\alpha x^{-(\alpha+1)} & x \geq x_m, \\ 0 & x < x_m, \end{cases} \quad (22)$$

where $x_m > 0$ sets the minimum length scale, and the exponent $\alpha > 0$ describes the distribution shape. The power-law form of this distribution means it is invariant to a scale transformation: $x' = \kappa x$. This implies Gabor

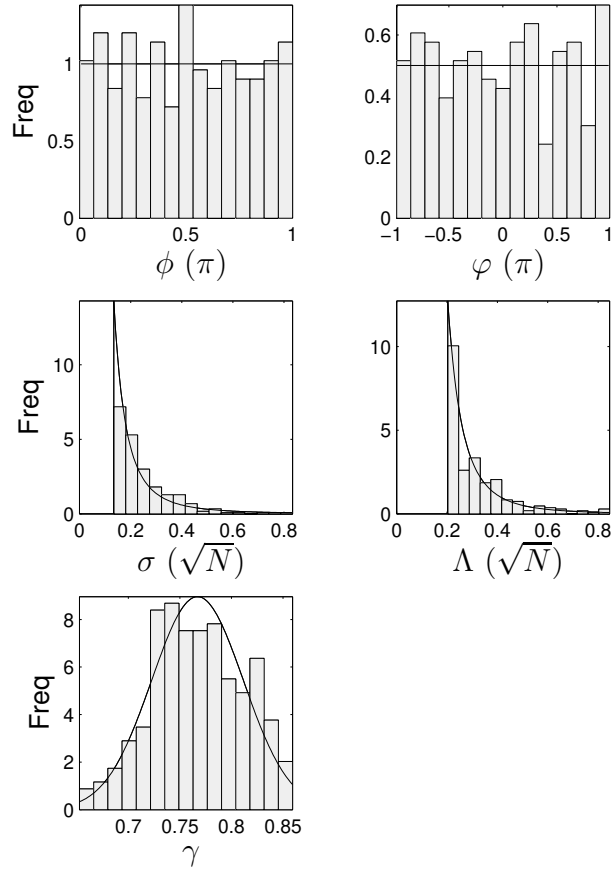


Figure 4: Histogram and fitted distribution (solid line) for each Gabor parameter of the learned dictionary in Fig. 2. To generate these plots 5 outliers with $\sigma > 2.8\sqrt{N}$ were removed from 256 data points.

Histogram	Distribution	Estimates	Sampler
ϕ	Uniform	$a = 0$ $b = \pi$	$\phi = a + (b - a)u$
φ	Uniform	$a = -\pi$ $b = \pi$	$\varphi = a + (b - a)u$
σ	Pareto	$\hat{\alpha} = 1.91$ $\hat{\sigma}_m = 0.134\sqrt{N}$	$\sigma = \hat{\sigma}_m u^{-(1/\hat{\alpha})}$
Λ	Pareto	$\hat{\alpha} = 2.59$ $\hat{\Lambda}_m = 0.203\sqrt{N}$	$\Lambda = \hat{\Lambda}_m u^{-(1/\hat{\alpha})}$
γ	Gaussian	$\hat{\mu} = 0.767$ $\hat{\sigma} = 0.045$	$\gamma = \hat{\mu} + \hat{\sigma}z$

Table 1: Univariate probability distribution and parameter estimates used to fit each histogram in Fig. 4. The sampler for each distribution is also shown: where u and z are drawn from standard uniform, and standard normal distributions, respectively.

functions in the learned dictionary have no characteristic length scale over the ranges $\hat{\sigma}_m < \sigma < \sigma_{\text{patch}}$ and $\hat{\Lambda}_m < \Lambda < \Lambda_{\text{patch}}$; where σ_{patch} and Λ_{patch} are maximum length scales determined by the patch size.

The histograms and fitted distributions in Fig. 4 and Table 1 represent the marginal distributions of the Gabor parameters. To see statistical dependencies in the joint probability distribution, I show scatter plots in Fig. 5 for each pair of correlated Gabor parameters with $p\text{-value} < 0.05$. It is seen that a strong correlation (line of best-fit slope=0.92) between σ and Λ has been learned. A weaker correlation (line of best-fit slope=0.18) has been learned between σ and γ . No other parameter pairs are found to exhibit statistically significant correlations.

4 Synthetic Dictionaries

Parametric models of the joint probability distribution of learned Gabor parameters are now estimated. The simplest parametric model is given by the graphical model (Bishop, 2006) shown in Fig. 6(a). In this case no correlations are modeled, and each parameter is independently sampled from its appropriate marginal distribution in Table 1.

Alternative parametric models can be constructed from the graphical

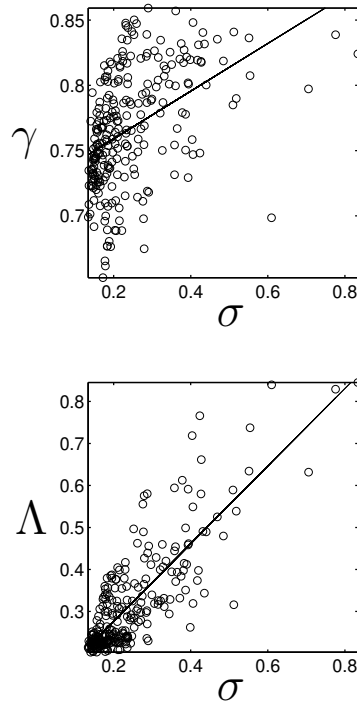


Figure 5: Scatter plot and line of best fit for each pair of correlated Gabor parameters with p-value <0.05 . (Top) Correlations between σ and γ , with line of best-fit slope=0.18. (Bottom) Correlations between σ and Λ , with line of best-fit slope=0.92. To generate these plots 5 outliers with $\sigma > 2.8\sqrt{N}$ were removed from 256 data points.

model shown in Fig. 6(b). In this case, I model the correlation in Fig. 5 (Bottom Panel) as $P(\Lambda, \sigma) = P(\Lambda|\sigma)P(\sigma)$; where the conditional dependency $P(\Lambda|\sigma)$ is depicted by the arrow in Fig. 6(b). I approximate this dependency using two alternative approaches. The first approach is to use a line-of-best-fit model where I sample σ from the Pareto distribution $\mathcal{P}(\sigma|\hat{\alpha}, \hat{\sigma}_m)$ using the sampler in Table 1, then generate a sample of Λ according to

$$\Lambda = a\sigma + b, \quad (23)$$

where $a = 0.92$ is slope of the line of best-fit to the data in Fig. 5 (Bottom Panel), and $b = \hat{\Lambda}_m - a\hat{\sigma}_m$ so that $\Lambda = \hat{\Lambda}_m$ when $\sigma = \hat{\sigma}_m$ in Eq. (23). The resulting scatter plot is shown in Fig. 7 (Middle Panel), and models $P(\Lambda|\sigma)$ as a delta-function: $P(\Lambda|\sigma) = \delta(\Lambda - a\sigma - b)$.

The second approach models $P(\Lambda, \sigma)$ using the Gaussian copula function (Embrechts, 2001). In this case, the dependency is included through a bivariate Gaussian $\mathcal{N}(0, \Sigma)$ with

$$\Sigma = \begin{pmatrix} 1 & \rho \\ \rho & 1 \end{pmatrix}, \quad (24)$$

by choosing the value of $\rho > 0$ (in Figs. 7 and 8, I chose $\rho = 0.9$). Samples (x_1, x_2) are then drawn from this distribution using $\mathbf{x} = \mathbf{A}\mathbf{z}$; where \mathbf{A} is the Cholesky decomposition of Σ , and $\mathbf{z} = (z_1, z_2)$ – with z_1 and z_2 each drawn from the standard univariate normal $\mathcal{N}(0, 1)$. Next, the samples are transformed to uniform marginal distributions using $(u_1, u_2) = (\Phi(x_1), \Phi(x_2))$; where Φ is the cumulative distribution function (CDF) for the standard univariate normal. Finally, samples of Λ and σ are obtained using $(\Lambda, \sigma) = (\tilde{\Phi}^{-1}(u_1), \tilde{\Phi}^{-1}(u_2))$; where $\tilde{\Phi}^{-1}$ is the inverse CDF for the Pareto distributions in Table 1. The resulting scatter plot is shown in Fig. 7 (Bottom Panel).

Synthetic dictionaries with statistical properties similar to those learned from natural images can now be generated by drawing samples from these parametric models. To find which dictionary better captures the statistical properties of natural images, I compare performance on image-patch reconstruction at different sparseness levels in Fig. 8. The sparseness norm for a single patch = $\sum_{\mathbf{r}} S(a(\mathbf{r})) / \sum_{\mathbf{r}} S(I(\mathbf{r}))$; and is averaged over all patches to get the mean sparseness norm, as explained in relation to Fig. 3. Results from the initial and learned dictionaries in Figs. 1 and 2 are shown as a comparison.

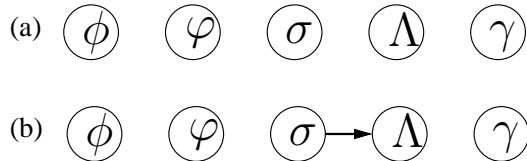


Figure 6: Two minimal graphical models of the joint probability distribution of learned Gabor parameters. (a) Model with no dependencies between Gabor parameters. (b) Model with the conditional dependency $P(\Lambda|\sigma)$ depicted by the arrow.

A dictionary corresponding to the graphical model in Fig. 6(a) is constructed by sampling the univariate distributions in Table 1. In this case there is no dependency between Λ and σ , as shown in Fig. 7 (Top Panel). In Fig. 8, it is seen that this uncorrelated dictionary leads to a significant increase in performance over the initial dictionary. The difference is the result of sampling the Gabor parameters σ , γ , and Λ from non-uniform distributions learned from natural image data.

Dictionaries corresponding to the graphical model in Fig. 6(b) include a correlation between Λ and σ . Sampling ϕ , φ , σ , and γ from the univariate distributions in Table 1, and using Eq. (23) to generate Λ , leads to a line-of-best-fit (LBF) correlated dictionary. The modeled dependency between Λ and σ is shown in Fig. 7 (Middle Panel). Sampling Λ and σ directly from the Gaussian copula leads to a copula-correlated dictionary, and the modeled dependency between Λ and σ is shown in Fig. 7 (Bottom Panel). In Fig. 8, it is seen that including the correlation between Λ and σ leads to a significant increase in performance over the uncorrelated dictionary; suggesting this correlation is crucial for generating good synthetic dictionaries. The Gaussian copula model does slightly worse than the line-of-best-fit model – despite making use of an extra parameter (given by the α parameter for the Pareto distribution over Λ).

Summary and Discussion

In this work, I constructed a parametric wavelet dictionary comprising a set of Gabor functions, and learned the joint probability distribution of the Gabor parameters from data consisting of natural images. The dictionary

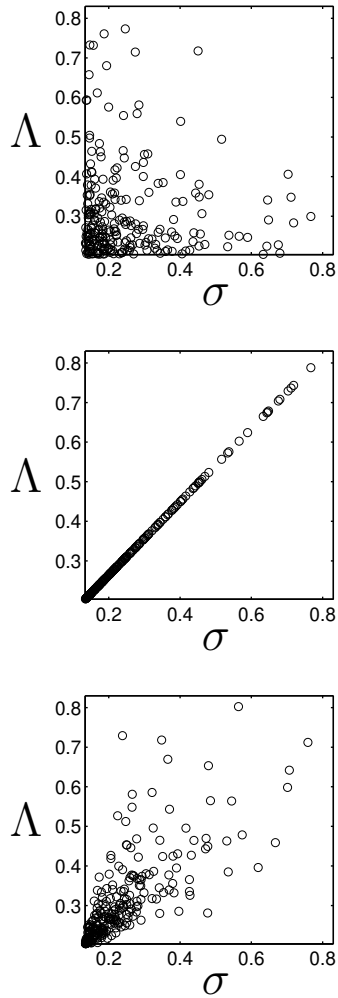


Figure 7: Scatter plots for σ and Λ sampled from different models of the statistical dependency in Fig. 5 (Bottom Panel). (Top) No dependency. (Middle) Line-of-best-fit dependency. (Bottom) Gaussian-copula dependency.

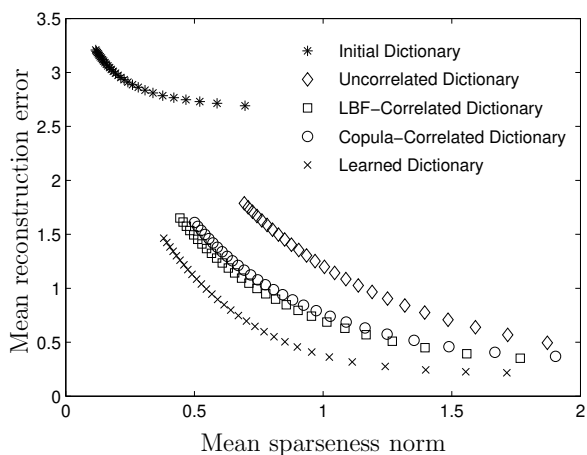


Figure 8: Mean reconstruction error for a set of 300 test-patch reconstructions at different sparseness levels (see text). Results are shown from using the dictionary of initial values from Fig. 1 (Asterisks), the learned dictionary from Fig. 2 (Crosses), and three synthetic dictionaries (Diamonds, Squares, Circles). The uncorrelated dictionary (Diamonds) is represented by the graphical model in Fig. 6(a), and has no modeled dependencies. Correlated dictionaries are represented by the graphical model in Fig. 6(b); and dependency between Λ and σ is modeled using either a line of best fit (Squares), or a Gaussian copula (Circles).

was constructed so that the set of Gabor functions uniformly tiled space. The learned Gabor parameter statistics resulted in a uniform tiling of orientation and phase, and a non-uniform tiling of receptive-field (windowing) size; spatial frequency; and aspect ratio. The joint probability distribution of learned Gabor parameters was shown to have a strong correlation between the receptive-field size and spatial frequency parameters.

I estimated three simple parametric models of the learned joint probability distribution, and constructed synthetic dictionaries from these models. A comparison of each synthetic dictionary on image-patch reconstruction performance showed that the two correlated dictionaries modeling the dependency between receptive-field size and spatial frequency outperformed the uncorrelated dictionary, and approached the performance of the learned dictionary. By virtue of having a parametric model for both the joint probability distribution and the wavelet dictionary, these synthetic dictionaries are fully parametric; and depend only on a handful of parameters. The work presented here generalizes approaches based on uniform wavelet parameter sampling, to wavelet parameters that are sampled from non-uniform distributions learned from natural image data – thereby adapting wavelets to the statistics of natural images. It would be interesting to see a detailed comparison between these two different approaches.

Comparing Gabor parameter statistics would be interesting for different classes of images, such as images of man-made environments versus images of natural scenes. For images of man-made environments, histograms of the orientation and receptive-field-size parameters are expected to be quite different to those presented here. Another application could be to use synthetic dictionaries as initializers for non-parametric learning algorithms. This might speed up convergence, and allow different local maxima of the likelihood to be explored by systematically varying the parameter statistics.

If dictionary statistics are found to be robust over different sparse coding schemes and different natural-image data sets, then the technique of learning the joint probability distribution of wavelet parameters from data may lead to further insight into efficient coding strategies, and to a better understanding of the function of simple cells in the primary visual cortex.

Acknowledgments

This work was supported by the U.S. Department of Energy; partly through the Center for Nonlinear Studies; and partly through the LANL/LDRD Pro-

gram projects 20090006DR, and 20130013DR.

Appendix

The partial derivatives required in Eqs. (18) and (19) are given here:

$$\frac{\partial g^T(\mathbf{r}, \mathbf{r}')}{\partial \phi(\mathbf{r})} = (\gamma(\mathbf{r})^2 - 1) \frac{\tilde{x}\tilde{y}}{\sigma(\mathbf{r})^2} g^T(\mathbf{r}, \mathbf{r}') - 2\pi \frac{\tilde{x}}{\Lambda(\mathbf{r})} h^T(\mathbf{r}, \mathbf{r}'), \quad (25)$$

$$\frac{\partial g^T(\mathbf{r}, \mathbf{r}')}{\partial \sigma(\mathbf{r})} = \left(\frac{\tilde{y}^2 + \gamma(\mathbf{r})^2 \tilde{x}^2}{\sigma(\mathbf{r})^3} \right) g^T(\mathbf{r}, \mathbf{r}'), \quad (26)$$

$$\frac{\partial g^T(\mathbf{r}, \mathbf{r}')}{\partial \gamma(\mathbf{r})} = -\frac{\gamma(\mathbf{r}) \tilde{x}^2}{\sigma(\mathbf{r})^2} g^T(\mathbf{r}, \mathbf{r}'), \quad (27)$$

$$\frac{\partial g^T(\mathbf{r}, \mathbf{r}')}{\partial \Lambda(\mathbf{r})} = \frac{2\pi \tilde{y}}{\Lambda(\mathbf{r})^2} h^T(\mathbf{r}, \mathbf{r}'), \quad (28)$$

$$\frac{\partial g^T(\mathbf{r}, \mathbf{r}')}{\partial \varphi(\mathbf{r})} = -h^T(\mathbf{r}, \mathbf{r}'), \quad (29)$$

where $g^T(\mathbf{r}, \mathbf{r}') = g(\mathbf{r}', \mathbf{r})$ is the transpose of $g(\mathbf{r}, \mathbf{r}')$, and $h^T(\mathbf{r}, \mathbf{r}') = h(\mathbf{r}', \mathbf{r})$ is the transpose of

$$h(\mathbf{r}, \mathbf{r}') = \exp\left(\frac{-\tilde{y}^2 - \gamma(\mathbf{r}')^2 \tilde{x}^2}{2\sigma(\mathbf{r}')^2}\right) \sin\left(2\pi \frac{\tilde{y}}{\Lambda(\mathbf{r}')} + \varphi(\mathbf{r}')\right), \quad (30)$$

and (\tilde{x}, \tilde{y}) are defined as in Eq. (5).

References

- Bell, A. J., & Sejnowski, T. J. (1995). An information-maximization approach to blind separation and blind deconvolution. *Neural Comp.*, *7*, 1129 – 1159.
- Bell, A. J., & Sejnowski, T. J. (1997). The “Independent Components” of natural scenes are edge filters. *Vision Res.*, *37*, 3327 – 3338.
- Bishop, C. M. (2006). *Pattern Recognition and Machine Learning*, Springer, U.S.A

- Daugman, J. G. (1988). Complete discrete 2-D Gabor transforms by neural networks for image analysis and compression. *IEEE Trans. Acoustics, Speech, Sig. Proc.*, *36*, 1169 – 1179.
- Daugman, J. G. (1989). Entropy reduction and decorrelation in visual coding by oriented neural receptive fields. *IEEE Trans. Biomed. Eng.*, *36*, 107 – 114.
- Durbin, R., & Mitchison, G. (1990). A dimension reduction framework for understanding cortical maps. *Nature*, *343*, 644 – 647.
- Embrechts, P., Lindskog F., & McNeil, A. (2001). Modelling dependence with copulas. *Handbook of Heavy Tailed Distributions in Finance*, Elsevier Science (2003).
- Field, D. J. (1994). What is the goal of sensory coding? *Neural Comp.*, *6*, 559 – 601.
- Field, D. J. (1999). Wavelets, vision, and the statistics of natural scenes. *Phil. Trans. R. Soc. Lond. A*, *357*, 2527 – 2542.
- Goldstein, T., & Osher, S. (2009). The Split Bregman Method for L1 regularized problems. *SIAM J. Im. Sci.*, *2*, 323 – 343.
- Horn, B. P. H. (1986). *Robot vision*, MIT Press.
- Hyvärinen, A., & Hoyer, P. (2000). Emergence of phase- and shift-invariant features by decomposition of natural images into independent feature subspaces. *Neural Comp.*, *12*, 1705 – 1720.
- Hyvärinen, A., Hoyer, P., & Inki, M. (2001). Topographic independent component analysis. *Neural Comp.*, *13*, 1527 – 1558.
- Hyvärinen, A., Hurri, J., & Hoyer, P. O. (2009). *Natural Image Statistics*, Springer-Verlag, London.
- Köster, U., & Hyvärinen, A. (2010). A two-layer model of natural stimuli estimated with score matching. *Neural Comp.*, *22*, 2308 – 2333.
- Lee, T. S. (1996). Image representation using 2D Gabor wavelets. *IEEE Trans. Pattern. Anal. Mach. Intell.*, *18*, 959 – 971.

- Lewicki, M. S., & Olshausen, B. A. (1999). Probabilistic framework for the adaptation and comparison of image codes. *J. Opt. Soc. Am. A*, *16*, 1587 – 1601.
- Linsker, R. (1986). From basic network principles to neural architecture: emergence of orientation selective cells. *Proc. Natl. Acad. Sci. USA*, *83*, 8390 – 8394.
- Marcelja, S. (1980). Mathematical description of the responses of simple cortical cells. *J. Opt. Soc. Am.*, *70*, 1297 – 1300.
- Mardia, K. V. (1962). Multivariate Pareto distributions. *Ann. Math. Stat.*, *33*, 1008 – 1015.
- Olshausen, B. A., & Field, D. J. (1996). Emergence of simple-cell receptive field properties by learning a sparse code for natural images. *Nature*, *381*, 607 – 609.
- Olshausen, B. A., & Field, D. J. (1997). Sparse coding with an overcomplete basis set: a strategy employed by V1? *Vision Res.*, *37*, 3311 – 3325.
- Olshausen, B. A., Sallee, P., & Lewicki, M. S. (2001). Learning sparse image codes using a wavelet pyramid architecture. *Ad. Neural Inform. Proc. Syst.*, *13*, 887 – 893.
- Olshausen, B. A., & Field, D. J. (2005). How close are we to understanding V1? *Neural Comp.*, *17*, 1665 – 1699.
- Sparsenet. Code and images available at <http://redwood.berkeley.edu/bruno/sparsenet>, courtesy of Bruno Olshausen.
- Swindale, N. V. (1996). The development of topography in the visual cortex. *Network: Comp. in Neural Syst.*, *7*, 161 – 247.
- Ullman, S. (1996). *High-level vision*, MIT Press.
- von der Malsburg, Ch. (1973). Self-organization of orientation sensitive cells in the striate cortex. *Kybernetik*, *14*, 85 – 100.